HHS Public Access

Author manuscript

Gene Ther. Author manuscript; available in PMC 2016 August 02.

Published in final edited form as:

Gene Ther. 2016 April ; 23(4): 380–392. doi:10.1038/gt.2016.11.

Exosome-associated AAV vector as a robust and convenient neuroscience tool

Eloise Hudry[1,2], **Courtney Martin**[1,2], **Sheetal Gandhi**[1,2], **Bence György**[2,3], **Deborah I. Scheffer**[3], **Dakai Mu**[2], **Steven F. Merkel**[4], **Federico Mingozzi**[5], **Zachary Fitzpatrick**[2], **Hemi Dimant**[6], **Marissa Masek**[6], **Tim Ragan**[6], **Sisareuth Tan**[7], **Alain R. Brisson**[7], **Servio H. Ramirez**[4], **Bradley T. Hyman**[1,2], and **Casey A. Maguire**[2,#]

[1]Alzheimer Research Unit, The Massachusetts General Hospital Institute for Neurodegenerative Disease, Charlestown, MA

[2]Department of Neurology, The Massachusetts General Hospital, and NeuroDiscovery Center, Harvard Medical School, Boston, USA

[3]Department of Neurobiology, Harvard Medical School, Boston, USA

[4]Department of Pathology and Laboratory Medicine, Temple University School of Medicine, Philadelphia, PA

[5]Genethon, Evry, France

[6]TissueVision, Inc., Cambridge, MA

[7]UMR-CBMN CNRS-University of Bordeaux, Pessac, France

Abstract

Adeno-associated virus (AAV) vectors are showing promise in gene therapy trials and have proven to be extremely efficient biological tools in basic neuroscience research. One major limitation to their widespread use in the neuroscience laboratory is the cost, labor, skill, and time intense purification process of AAV. We have recently shown that AAV can associate with exosomes (exo-AAV) when vector is isolated from conditioned media of producer cells, and the exo-AAV is more resistant to neutralizing anti-AAV antibodies compared to standard AAV. Here we demonstrate that simple pelleting of exo-AAV from media via ultracentrifugation, results in high-titer vector preparations capable of efficient transduction of central nervous system (CNS) cells after systemic injection in mice. We observed that exo-AAV is more efficient at gene delivery to the brain at low vector doses relative to conventional AAV, even when derived from a serotype that does not normally efficiently cross the blood brain barrier. Similar cell types were transduced by exo-AAV and conventionally purified vector. Importantly, no cellular toxicity was noted in exo-AAV transduced cells. We demonstrated the utility and robustness of exo-AAV-mediated gene delivery by detecting direct GFP fluorescence after systemic injection, allowing 3-dimensional

[#]Correspondence should be addressed to: Casey A. Maguire, Ph.D., Neuroscience Center, The Massachusetts General Hospital, Building 149, 13th Street, Charlestown, MA, 02129 USA. Phone 617-726-5725, Fax 617-724-1537, ; Email: cmaguire@mgh.harvard.edu

reconstruction of transduced Purkinje cells in the cerebellum using *ex-vivo* serial 2-photon tomography. The ease of isolation combined with the high efficiency of transgene expression in the CNS, may enable widespread use of exo-AAV as a neuroscience research tool. Furthermore, the ability of exo-AAV to evade neutralizing antibodies while still transducing CNS after peripheral delivery is clinically relevant.

INTRODUCTION

Gene therapies applied to neurodegenerative diseases have encountered an increased interest over the past few years, a trend closely associated with promising clinical trial results using adeno-associated vectors (AAV) in multiple inherited pathological contexts (1–6). The recent characterization of several novel AAV serotypes has demonstrated that a single intravenous injection in adult mice leads to transduction of neural cells throughout the entire central nervous system (7, 8). Considering the excellent safety profile of AAV, the implications of those findings are of great importance in the field, paving the way toward a non-invasive and remarkably efficient method to broadly express novel genetic therapeutic targets into the brain after peripheral administration.

Due to their remarkable ability to transduce a large percentage of astrocytes, neurons, and endothelial cells in the brain and spinal cord, AAV has also become a favored tool of neuroscientists. Offering a unique opportunity to precisely manipulate gene expression with time and spatial resolution, these vectors have been extensively used over the years to perform genetic manipulations aimed at further deciphering the fundamental bases of neurobiology such as neuronal circuitry, neuron/glia functional interaction or molecular profiling (9–16). However the skill and labor required to process and purify AAV vectors is often beyond the means of basic science laboratories. Alternatively, AAV vectors can be purchased from academic cores or companies, often at significant cost. Typical AAV is produced by transient triple transfection of 293 cells, extraction of the vector from the cell lysate, and purification of the vector using density gradient ultracentrifugation, anion-exchange or affinity chromatography, and finally desalting and concentration using dialysis or ultrafiltration devices.

We previously reported that a portion of AAV isolated from media is associated with extracellular vesicles (EVs) (17), often classically termed exosomes. In a follow-up study we showed that this exosome-associated AAV (exo-AAV) resisted neutralizing anti-AAV antibodies (a major clinical barrier) *in vitro* and *in vivo* compared to conventional AAV and that we could enhance exo-AAV transduction in the brain by displaying targeting peptides on the EV surface[18].

Here we show that exo-AAV, a novel gene transfer tool that can be easily produced in five days after a simple high-speed centrifugation step, is a highly efficient and convenient gene delivery agent for neuroscience research. While the overall tropism of exo-AAV9 is as broad as its conventional counterpart, targeting multiple neural cell types throughout the central nervous system, it generally outperforms AAV9 and leads to significantly higher percentages of astrocytes and neurons expressing a reporter gene. Importantly, when using an AAV

serotype with limited capacity to cross the blood brain barrier, we show that the presence of exosomes enhances the transduction of the cerebral tissue at low doses.

RESULTS

Exo-AAV9-CBA-GFP retains AAV9-CBA-GFP's capacity to cross the blood brain barrier, widely transduces the neural tissue, and leads to fluorescence directly detectable by *in vivo* and post-mortem 2-photon imaging

In this study we used exo-AAV9 isolated in the 100,000×*g* fraction (see methods for details). We were able to confirm the presence of viral particles inside or associated with the surface of EVs in exo-AAV by Cryo-EM (Supplementary Fig. 1). As expected, non-enveloped particles were observed following a conventional protocol of AAV preparation and purification. We also compared the relative protein content in iodixanol purified AAV9 and exo-AAV9 preparations. A fixed dose (6×10^{10} g.c.) of each preparation was loaded onto an SDS PAGE gel and after electrophoresis stained to visualize total protein. As expected, the highly purified iodixanol preparation consisted of mainly the three capsid proteins (VP1, VP2, and VP3) (Supplementary Fig. 2). In contrast, the exo-AAV9 sample contained many more non-AAV proteins (Supplementary Fig. 2). Likely, many of these are exosome-associated proteins such as transmembrane receptors, although some may be co-precipitating proteins from the conditioned media, such as bovine serum albumin (BSA), a known contaminant in exosome preparations (18).

To characterize the transduction properties of exo-AAV in the CNS at a cellular level, equivalent doses of self-complementary (sc) AAV9-CBA-GFP and exo-AAV9-CBA-GFP genome copies (1.5×10^{11} g.c/mouse) were injected in the lateral tail vein of wild-type immunocompetent BALB/c mice and the animals were euthanized after 3 weeks. As expected, hepatocytes in the liver were primarily transduced in the periphery (Supplementary Fig. 3), while an evaluation of the transduction profiles of exo-AAV9 and AAV9 showed that both preparations also efficiently target the central nervous system (brain and spinal cord, Fig. 1). The signal detected after immunolabeling for GFP was largely spread across the entire cerebral tissue and was present throughout large brain areas such as cortex, striatum, hippocampus and cerebellum (Fig. 1a). Even though the signal intensity appears to be higher after exo-AAV9 injection as compared with AAV9, no significant difference in the overall distribution of the fluorescence was observed. Similar to conventional AAV9, GFP signal was detected within the spinal cord of exo-AAV9 injected mice as well (Fig. 1b). We conclude that exo-AAV9 does not significantly alter the transduction profile observed with the corresponding conventional AAV9, and keeps its efficacy at crossing the blood brain barrier to achieve widespread expression of reporter gene throughout the entire nervous system.

Considering the increased interest in using genetically encoded fluorescent reporters to monitor dynamic processes *in vivo* in live animals or the advantage of imaging fluorescent proteins applicable to novel high throughput microscopy techniques, we also determined if the GFP fluorescent signal driven by peripherally injected exo-AAV could be detected in the mouse brain without immunolabeling (the conventional approach). To this end, BALB/c mice were injected i.v. with 7×10^{11} g.c. of sc-exo-AAV9-CBA-GFP. Four weeks later, a

cranial window was placed above the somatosensory cortex in order to visualize GFP fluorescent cells by 2-photon imaging in the living animal. Sparse GFP positive astrocytes were detected by two-photon *in vivo* imaging (Fig. 2a: example of transduced astrocyte endfeet). In addition, ex-vivo imaging of direct GFP signal could be achieved by serial two-photon (STP) tomography, leading to a 3 dimensional overview of chosen cerebral volumes. As an example, transduced Purkinje neurons, astrocytes and endothelial cells were clearly distinguished in the cerebellum (Fig. 2b, c and Movies 1 and 2).

Exo-AAV9 and conventional AAV9 target multiple neural cell types in the brain, a tropism dependent upon the routes of administration

In order to precisely identify the different cell types transduced after intravenous injection of exo-AAV9 and AAV9, co-immunostainings were performed between GFP and specific markers of various neural cell types and sub-types. We observed that the vast majority of GFP positive cells were astrocytes, identified by the marker Glutamine Synthetase (GS), followed by NeuN positive neurons (Fig. 3a, b). Both parenchymal astrocytes as well as astrocytic endfeet were evenly targeted, with no greater preference for cells located in the vicinity of blood vessels (Fig. 3a and Supplementary Fig. 4a), even though the vascular endothelium was more efficiently targeted by exo-AAV9 as opposed to AAV9 (Supplementary Fig. 4b). Among neuronal cells, excitatory as well as inhibitory neurons (respectively identified by the markers CamKII and GAD67) expressed GFP (Fig. 4a, b). Of relevance in specific neuropathologic contexts, few dopaminergic neurons positive for the Tyrosine Hydroxylase were detected in the substantia nigra of exo-AAV9 injected animals but could not be observed with AAV9 (Fig. 4c) at the administered dose. In addition, numerous GFP positive Purkinje cells were also observed in the cerebellum (Fig. 4d) and ChAT positive motor neurons were detected in the spinal cord (Fig. 4e). Besides neurons and astrocytes, sparse transduced oligodendrocytes were also observed in the corpus callosum of both exo-AAV9 and AAV9 injected mice (Fig. 3b). By contrast, no microglial cells expressing GFP was detected after injection of either vector (Fig. 3b). Overall, these results confirm that exo-AAV9 and standard AAV9 share comparable tropism profiles in the central nervous systems after peripheral injection, with the exception of the additional transduction of dopaminergic neurons by exo-AAV9.

Of interest, we also found that several important components of both visual and auditory systems were transduced with exo-AAV9. In the retina, GFP fluorescent signal was observed in the inner nuclear layer (INL) and in the ganglion cell layer (GCL) after exo-AAV9 injection, whereas few transduced cells were detected with AAV9 (Supplementary Fig. 5a). In addition, we were able to detect transduction of inner hair cells and supporting cells in both the cochlea and vestibule (Supplementary Fig. 5b).

For some research, targeted transduction of specific structures in the brain is required as opposed to widespread expression. We therefore tested the transduction capabilities of exo-

Movie 1. Serial 2-photon images of direct GFP expression and Dextran-Texas Red filled blood vessels throughout the cerebellum from mice injected i.v. with exo-AAV9-GFP.
Movie 2. 3D reconstruction of the exo-AAV9-GFP transduced cerebellum imaged by serial two-photon (STP) tomography showing the overall direct GFP signal throughout the tissue as well as individual transduced cells.

AAV9 after direct intraparenchymal injections of both sc-AAV9-CBA-GFP and sc-exo-AAV9-CBA-GFP in wild-type mice, targeting either the sensorimotor cortex or the striatum (3.2×10^9 g.c./injection site). After three weeks, a majority of GFP positive cells could be identified as neurons, with only a sparse expression in cortical astrocytes (Supplementary Fig. 6). In the striatum, almost all transduced cells also expressed the neuronal marker NeuN (Supplementary Fig. 6).

Intravenous delivered exo-AAV9 outperforms conventional AAV9 in transducing astrocytes and neurons

In order to have a quantitative evaluation of the gene transfer efficacy of exo-AAV9 and AAV9 delivered systemically, an unbiased stereological analysis of the percentages of astrocytes and neurons, respectively identified by the markers Glutamine Synthetase and NeuN, was performed in the cortex, striatum and hippocampus. GFP/NeuN double positive cells showed that exo-AAV9 generally out-performed conventional AAV9, reaching 5.11±0.28% of transduced neurons in the cortex and 5.31±0.27% in the striatum as opposed to 2.87±0.12% and 2.79±0.18%, respectively, with AAV9 (Mann Whitney test, $p<0.0001$ for both cortex and striatum, Fig. 5a). In the hippocampus, the transduction efficacy varied between each cornu ammonis (CA) subfields and the dentate gyrus, with a greater signal detected in CA3 (Fig. 5b). We quantified 5.45±0.57% of GFP expressing neurons in CA1/2 (AAV9: 2.66±0.46%; Mann Whitney test, $p=0.003$), 7.93±0.54% in CA3 (AAV9: 4.37±0.84%; Mann Whitney test, $p=0.0104$) and 6.19±0.79% in the dentate gyrus (AAV9: 3.15±0.34%, Mann Whitney test, $p=0.015$) after injection with exo-AAV9. Overall the transduction level of neurons was 1.9 fold higher after intravenous injection of exo-AAV9 as compared to the corresponding conventional AAV9. The percentages of exo-AAV9 targeted astrocytes, identified as cells positive for both GFP and Glutamine Synthetase, reached 15.37±0.7% and 12.64±0.91% respectively in the cortex and striatum, which was significantly higher than the efficacy observed with the conventional AAV9 (cortex: 9.3±1.2% and striatum: 7.02±1.05%; Mann Whitney test, $p=0.0234$ for the striatum and $p=0.007$ for the cortex) (Fig. 6a, b). A similar trend was observed in the hippocampus but did not reach statistical significance (AAV9: 5.56±1.41% and exo-AAV9: 8.91±1.74%; Mann Whitney test, $p=0.18$, Fig. 6c). Overall, our stereology-based analysis showed that peripherally administered conventional AAV9 vector only reaches about 63% of the efficacy of exo-AAV9 to transduce astrocytes.

Brain transduction is enhanced for exo-AAV8 vector

To evaluate the contribution of the vesicle portion of the exo-AAV system in the CNS transduction efficacy after i.v. injection, we chose AAV8 as this serotype is widely used in direct intracerebral gene delivery, although its ability to cross the BBB is reported to be less efficient than AAV9 (7). We have previously demonstrated that exo-AAV9 is more resistant to IVIg than conventional AAV9 vector (19). Similarly, we found exo-AAV8 to have a higher resistance to neutralizing antibodies than conventional AAV8 (Supplementary Fig. 7), suggesting that EVs can also protect AAV8 from neutralization. Specifically, while conventional AAV8 was neutralized by 50% at 0.2 mg/ml IVIg, exo-AAV8 transduction was reduced by this level at a 7.9-fold higher dose of IVIg (1.57 mg/ml) (Supplementary Fig. 7). Next we compared the kinetics of transgene expression by systemically injecting female

BALB/c mice with 5×10^{10} g.c. of conventional ss-AAV8 or ss-exo-AAV8 encoding firefly luciferase (FLuc) driven by the CBA promoter. Non-invasive, whole-body bioluminescence imaging (BLI) was performed weekly for 4 weeks to detect FLuc-associated bioluminescent signal in mice and we specifically analyzed the signal intensity in the head and the liver regions (representative images, Fig. 7a). Remarkably, at 1 week post transduction, the FLuc signal emanating from the head region was 15-fold higher in the exo-AAV8 group than the standard AAV8 group (p=0.003, t-test, Fig. 7b). Imaging for 28 days revealed a consistent higher signal in the head region for exo-AAV8 over standard AAV8, while the signal slowly decreased over time in the liver (Fig. 7c and d). To confirm the *in vivo* BLI results, another cohort of BALB/c mice were injected i.v. with 5×10^{10} g.c. of ss-exo-AAV8-CBA-FLuc or conventional ss-AAV8-CBA-FLuc and 4 weeks later, mice were sacrificed, perfused with PBS and brain homogenates analyzed by a luciferase assay in a luminometer. Consistent with the BLI data, the luciferase levels were approximately 4-fold higher in the exo-AAV8 group than the AAV8 group (p=0.006, t-test, Fig. 7e).

Finally, to analyze the cell types transduced by exo-AAV8, BALB/c mice were injected with 4×10^{11} g.c. of sc-AAV-CBA-GFP in either exo-AAV8 or conventional AAV8 formats. Mice were sacrificed two weeks post injection and immunofluorescence staining for GFP was performed. Qualitatively, AAV8 and exo-AAV8 appeared to transduce cells of similar morphology resembling astrocytes, neurons, and vascular cells (possibly endothelial cells as observed with AAV9/exo-AAV9, or pericytes), with no evidence of enhanced transduction efficiency with exo-AAV8 (Fig. 8a, b), in contrast to the BLI experiments. To explore whether the discrepancy between the data using the FLuc reporter and GFP reporter had a dose-related component, we injected mice with three doses (5×10^{10}, 3×10^{11}, and 1×10^{12} g.c.) of either AAV8-CBA-GFP or exo-AAV8-CBA-GFP. We also used a single-stranded (ss) GFP genome, which matches the ss FLuc genome. This reduces the efficacy of detection compared to sc vector so we used anti-GFP immunoblots to detect GFP in the brain of mice. Two weeks post-injection, mice were sacrificed. First we performed qPCR analysis on genomic DNA isolated from brain homogenates. We observed an increase (1.8-fold) in AAV genome copies in the brain of mice injected with exo-AAV8 at the lower doses, and no increase at the highest dose (Fig. 8c). We next performed western blotting for GFP at the lowest dose of vector (5×10^{10}g.c.), which was identical to the dose used in the FLuc experiments. We observed a faint, yet enhanced GFP immunoreactive band in mice in exo-AAV8 injected mice (Fig. 8d). Normalization to GAPDH revealed a 3.5-fold increase in GFP immunostaining with exo-AAV8 compared to AAV8 (p=0.15, Fig. 8e). Based on these data it appears that exo-AAV8 enhances transduction at lower doses of vector in the context of a single stranded genome.

exo-AAV outperforms standard AAV at crossing a model of the blood-brain barrier

It is likely that multiple mechanisms regulate the enhanced transduction efficiency of exo-AAV over standard AAV in the brain; however, these mechanisms are poorly understood and challenging to address *in vivo*. One possible mechanism is that exo-AAV may also access the brain parenchyma by negotiating the blood-brain barrier (BBB) more efficiently than conventional AAV. In order to determine if the enhanced transduction efficiency of exo-AAV may be related to more permissive interactions with the brain microvasculature, an *in vitro*

model of the BBB was employed. To this end, bEnd.3 cells (mouse brain endothelial cells were grown to confluence on collagen-coated cell culture inserts, allowing time for a baseline transendothelial electrical resistance ($\geq 40 \Omega cm^2$) to be established (20). The expression of unique tight junction protein complexes generate a physical barrier that impedes the movement of small, charged molecules. After assessing barrier integrity by measuring electrical resistance, conventional AAV8, AAV9, or exo-AAV8 or exo-AAV9 were suspended in media and dispensed into the upper chamber of cell culture inserts containing the bEnd.3 endothelial monolayer. After 24 hours, media was collected from the lower chamber and analyzed by qPCR for the presence of AAV genomes. Strikingly, we observed exo-AAV9 and exo-AAV8 to have a 9.3-fold (p=0.002, t-test) and 4.3-fold (p=0.088, t-test) increase in transendothelial action compared to their standard AAV counterparts, respectively (Fig. 9).

DISCUSSION

Improvements of existing vector expression cassettes, discovery of novel serotypes, and engineering of new capsids have made AAV vectors remarkable tools for neuroscience research as well as clinical applications. For example, AAV-mediated gene delivery to the CNS has been used to map neural circuits (13), characterize various neuronal sub-population *in vivo* (12, [14]), address functional connectivity between neurons and astrocytes (11), determine gene function using CRISPR-Cas9 (9, [10]), and mediate spatial and temporal control of transgene expression in transgenic mice using the Cre-*loxP* approach (16). In general, research grade AAVs are extremely expensive to purchase from a company, especially when multiple constructs are required, such as for mutagenesis studies. Much of this cost is due to the high degree of technical skill required to isolate and purify AAV.

Conventional AAVs are isolated from cell lysates and subjected to subsequent purification via iodixanol or cesium chloride density ultracentrifugation or affinity based chromatography and finally dialysis of the vector (21, [22]). These are labor intense and technically challenging procedures, which take at least 6–7 working days from plating cells to storage of the vector. Because it only takes 5 working days for exo-AAV preparation and requires only simple ultracentrifugation of media for isolation, exo-AAV should be more accessible to most neuroscience laboratories compared to conventionally purified AAV. This simplicity combined with the observation that exo-AAV can be isolated at comparable titers to conventional AAV as well as superior transduction performance, make exo-AAV a convenient and effective CNS tool. One argument concerning the use of exo-AAV is that they are not as highly purified as conventional AAV vectors, potentially containing nucleic acids such as miRNA and proteins as other exosome preparations (23–[25]). However, it is likely that any biological effects from these components should be transient, especially after peripheral delivery in which a minimal amount will reach the CNS. In the present study, we did not observe any morphological differences in transduced cells with exo-AAV compared to conventional AAV. However, one should always use a control exo-AAV vector in experiments as a control AAV vector would be used in conventional AAV experiments expressing a gene of interest.

We demonstrated the efficiency of exo-AAV in the CNS by detecting direct GFP fluorescence after i.v. injection of exo-AAV in a living animal by 2-photon imaging (without previous immunostaining). This finding may be of great interest in particular to label and image isolated astrocytes in the cortical mantel for dynamic functional analyses such as calcium recording, especially within individual processes that undergo calcium transients based on subtle changes within the microenvironment (26). Similarly, the direct GFP fluorescence was suitable to perform post-mortem serial two-photon (STP) tomography imaging, a powerful technology that allows 3 dimensional reconstructions of large brain volumes (27). As systemically delivered exo-AAV (or AAV) provides widespread neural transduction throughout the entire brain, the imaging capability of STP tomography could should allow rapid and comprehensive assessment of morphological effects of specific genetic modifications in neurons, astrocytes, and endothelial cells. It should be noted that typically, transduction of brain by systemically administered AAV is monitored by immunofluorescence staining with primary and secondary antibodies, a several-days process.

The present study used a sc-AAV-CBA-GFP reporter system to establish the transduction profile of exo-AAV9 at a cellular level across the CNS and PNS, using various combinations with specific cellular markers. Astrocytes were primarily targeted, reaching about 12% of transduction throughout the entire brain at the relatively low dose examined (1.5×10^{11} g.c./mouse, ~7.5×10^{12} g.c./kg). Besides the retina, which has been previously reported to be targeted by conventional AAV9 (28), we also made the striking observation that vestibular and cochlear hair cells were transduced in adult mice after i.v. injection with standard or exo-AAV9. To our knowledge this has never been reported after systemic injection of AAV vector. Conventionally, virus vectors are injected directly into the cochlea via cochleostomy or round window membrane (29), a rather invasive procedure. While the transduction of cochlear hair cells appears low after i.v. injection under the tested dose and conditions here, it demonstrates the feasibility of this route of administration, which may be further improved by injecting the vectors in one of the facial arteries connected to the labyrinthine artery. Of note, while the present work characterizes the transduction profile of exo-AAV9 using a ubiquitous promoter (CBA), which concomitantly leads to the expression of GFP in many different cell types as well as in the periphery (in the liver), one can utilize a cell-specific promoter in order to restrict the expression of the transgene in a specific cellular population.

In vivo data from this study reveal that exo-AAV produced in 293T cells can enhance transduction efficiency in the CNS compared to standard AAV; however, the mechanisms that permit exo-AAV to achieve this effect are currently unknown. Data presented in previous studies suggest that both EVs and AAV alone can traverse the blood-brain barrier (BBB) after intravascular administration (7, 8, 30, 31). Furthermore, another report specifically observed that EVs derived from 293T cells are distributed to the brain after intravascular injection (32). Therefore, exo-AAV may transduce a greater number of astrocytes and neurons in the brain by evading the blockade typically imposed by the BBB more efficiently than AAV alone. Using an *in vitro* BBB model, we have shown that exo-AAV outperforms standard AAV at crossing a monolayer of brain endothelial cells. It remains to be determined whether AAV separates from the EV after encountering the bEnd.3 monolayer and crosses the endothelium as a “naked” particle, or if the entire exo-AAV

complex negotiates its way across the endothelial barrier. Addressing these possibilities will be the focus of future investigations. Nonetheless, the results of this assay suggest that the difference in efficacy we observed *in vivo* between AAV and exo-AAV may be attributed, at least in part, to a higher potential for enveloped particles to engage the brain endothelium when compared to standard AAV. Interestingly, AAV8 vectors appear to penetrate the BBB less efficiently than AAV9 (7), yet our *in vivo* bioluminescence analyses have shown that exo-AAV8 exhibits greater transduction of parenchymal brain cells than conventional AAV8. This may suggest that the lipid envelop of 293T-derived EVs possesses dynamic properties that allow AAV8 to overcome unknown impediments in transduction of CNS after i.v. injection (e.g. penetrating the BBB). One possible explanation for this result may be that during the production of exo-AAV, 293T cells are able to pack multiple AAV vectors within a single EV as observed by Cryo-EM. This could allow more than one AAV capsid to cross the BBB after interacting with only a single exo-AAV. However, the benefit of packaging multiple capsids per EV may only help AAV vectors to access the CNS by subverting impedance at the BBB, while properties of the specific AAV serotype may ultimately limit the efficiency of transduction in the brain. As observed in Figure 8, the enhancement with exo-AAV8 was apparent at lower single stranded vector doses, which could be overcome by using a more robust expression vector in the self-complementary genome or increasing the dose of single stranded vector. Perhaps at lower doses, exo-AAV8 introduces a greater number of AAV vectors, or binds to a higher affinity cellular receptor, which can be overcome higher doses or the more efficient self-complementary genome. In any case, the ability to enhance gene delivery at lower vector doses is an attractive characteristic for clinical use.

Considering the significant percentage of AAV seropositivity among the human population (33, [34]), achieving transduction of CNS after systemic injection in the presence of neutralizing antibodies is a major challenge with current AAV vectors. We have previously demonstrated that iv injected exo-AAV could transduce CNS after pre-injection of human intravenous immunoglobulin, as measured by a bioluminescent reporter transgene (19). As this is an important observation with clinical implications, in this study we thoroughly characterized the transduction profile in the brain of exo-AAV9. Importantly, the present experiments were performed in naive mice not previously exposed to AAV or passively injected with human antibodies. Thus in the presence of anti-AAV antibodies, exo-AAV is expected to greatly outperform standard AAV at CNS transduction, which has clinical relevance.

In conclusion, systemic injection of exo-AAV vectors leads to robust transduction of important CNS target cells (neurons, astrocytes, endothelial cells). The ease of isolation combined with the antibody shielding feature, makes exo-AAV an attractive and cost-effective tool for basic CNS research as well as a potential gene therapy delivery system.

Materials and Methods

Cell Culture

Human 293T and bEnd.3 (mouse brain endothelial) cells were obtained from the American Type Culture Collection (Manassas, VA). Both cell types were cultured in high glucose

Dulbecco's modified Eagle's medium (Life Technologies, Grand Island, NY) supplemented with 10% fetal bovine serum (Sigma, St Louis, MO), 100 U/ml penicillin, and 100 μg/ml streptomycin (Life Technologies) in a humidified atmosphere supplemented with 5% CO2 at 37°C.

Conventional AAV and exo-AAV production

AAV vectors and exo-AAV were produced in 293T cells as previously described (17). Briefly, a triple transfection of AAV-CBA-GFP and helper plasmids was performed using the calcium phosphate method in ten 15 cm dishes. Standard AAV vectors were extracted from cell lysates and purified by iodixanol density gradient ultracentrifugation. Next, iodixanol was removed and vector concentrated using Amicon Ultra 100 kDa molecular weight cutoff (MWCO) centrifugal devices (Millipore, Billerica, MA) and phosphate buffered saline (PBS) and finally filtered through a 0.22 um Millex-GV Filter Unit (Millipore).

For exo-AAV, media was changed to EV-free 2% FBS the day after transfection. At 72 h post transfection, media was harvested. Cell debris and apoptotic bodies were removed by sequential, 10 min 300 × g and 2000 × g centrifugations, respectively. The supernatant containing exo-AAV was then centrifuged at 20,000 × g for 1 h to deplete larger microvesicles. Next, the remaining media was centrifuged at 100,000 × g for 1 hour using a Type 70 Ti rotor in a Optima™ L-90K ultracentrifuge (both Beckman Coulter, Inc., Indianapolis IN). The resulting pelleted material was resuspended in PBS. Both exo-AAV and standard AAV preparations were stored at −80°C until use. For immunofluorescence analysis of transduced cell types we used a self-complementary (sc) AAV construct encoding eGFP driven by the hybrid CMV-enhancer/chicken beta actin (CBA) promoter. sc-AAV-CBA-GFP is used throughout the study unless otherwise indicated as it leads to much more robust levels of transgene expression in the CNS compared to single stranded (ss) AAV vectors after i.v. injection (35). In some experiments with AAV8 and exo-AAV8 we used a ss AAV-CBA-eGFP construct. In bioluminescence experiments comparing AAV8 and exo-AAV8 we used a ss AAV vector encoding firefly luciferase (FLuc) driven by the CBA promoter. To ensure accurate titration of exo-AAV which contains protein and lipids, we purified AAV genomes using High Pure Viral Nucleic Acid Kit (Roche, Indianapolis, IN). This kit contains detergents and proteinase K to degrade and lyse membraned viruses and is also certified to remove PCR inhibitors. Before kit purification, plasmid DNA from the transfection was removed by mixing 5 μl of the exo-AAV samples with 1 μl DNase I, 5 μl 10× buffer, and 39 μl water. Samples were incubated 1 h at 37°C and then Dnase I was inactivated at 75°C for 15 min. Next, AAV and exo-AAV preparations were titered using a quantitative TaqMan PCR that detects AAV genomes (polyA region of the transgene cassette) was performed as previously described (3).

AAV and exo-AAV yields are very similar, consistently within 2-fold of one another. For ss vectors the titers and yields range from 8×10^{12}– 3×10^{13} g.c./ml and 4×10^{12}–1×10^{13} g.c., for AAV and exo-AAV respectively. For sc vectors the titers and yields range from 1×10^{12}–8×10^{12} g.c./ml and 1×10^{12}–6×10^{12} g.c., for AAV and exo-AAV respectively.

Cryo-electron microscopy

Aliquots (4 μL) of AAV1 or exo-AAV 1 stocks were deposited on electron microscopy (EM) grids coated with a perforated carbon film. After draining the excess liquid with a filter paper, grids were quickly plunged into liquid ethane and mounted onto a Gatan 626 cryoholder. Cryo-TEM observation was performed with a Tecnai F20 (FEI) microscope operated at 200 kV. The images were recorded with an USC1000-SSCCD camera (Gatan).

Animals and tail vein injection

All animal experiments were approved by the Massachusetts General Hospital Subcommittee on Research Animal Care following guidelines set forth by the National Institutes of Health Guide for the Care and Use of Laboratory Animals. Female BALB/c mice aged 6–8 weeks were purchased from Jackson Laboratory (Bar Harbor, ME). For tail vein injections of AAV and exo-AAV, mice were placed into a restrainer, (Braintree Scientific, Inc., Braintree, MA). Next the tail was warmed in 40°C water for 30 seconds, before wiping the tail with 70% isopropyl alcohol pads. A 100–300 μl volume of vector (~7.5×10^{12} g.c./kg, diluted in PBS) was slowly injected into a lateral tail vein, before gently finger clamping the injection site until bleeding stopped.

Stereotactic intraparenchymal injections

Stereotactic intracortical injections of AAV9 or exo-AAV9 were performed as described previously (36). Animals were anesthetized by intraperitoneal injection of ketamine/xylazine (100mg/kg and 50mg/kg body weight, respectively) and positioned on a stereotactic frame (Kopf Instruments). Injections of vectors were performed in either the somatosensory cortex or in the striatum with 3μl of viral suspension using a 33-gauge sharp needle attached to a 10-μl Hamilton syringe (Hamilton Medical), at a rate of 0.1 μl/minute. Stereotactic coordinates of injection sites were calculated from bregma (Cortex coordinates: anteroposterior −1 mm, mediolateral ± 1mm and dorsoventral −1mm; Striatum coordinates: anteroposterior +0.5mm, mediolateral ± 2.5mm and dorsoventral −2.5mm).

Cranial window implantation and in vivo multiphoton imaging

Three weeks after intravenous injection of exo-AAV9-CBA-GFP (self-complementary genome) (7×10^{11}gc/mouse), the mice were anesthesized with isoflurane (1–1.5%) and a cranial window was implanted. After removing the skull, the dura matter was removed with gin forceps in order to expose the brain parenchyma and topically apply SR101 for 40 minutes to label astrocytes. The window was then closed a glass coverslip of 8mm diameter (as described previously (37, [38]). For imaging, a warm paraffin wax ring was built along the border of the window to create a well of water for the dipping objective.

For *in-vivo* imaging, an Olympus FluoView FV1000MPE multiphoton laser-scanning system mounted on an Olympus BX61WI microscope and an Olympus 25× dipping objective (NA=1.05) were used. A DeepSee Mai Tai Ti:sapphire mode-locked laser (Mai Tai; Spectra-Physics) generated two-photon excitation at 860 nm, and detectors containing three photomultiplier tubes (Hamamatsu, Ichinocho, Japan) collected emitted light in the range of 420–460, 495–540, and 575–630 nm. Mice were placed on the microscope stage and heated using a heating pad and feedback regulation from a rectal temperature probe

(Harvard apparatus). Z-series (127μm × 127μm, 2μm steps, depth of about 200μm, 512 × 512 pixels) were taken. Laser power was adjusted as needed according to the brightness of the imaging fields.

Ex vivo Serial 2-photon tomography

To directly detect the GFP fluorescent signal *ex vivo* (without previous immunostaining) and perform high-speed imaging of the entire cerebellum, a dose of 7×10^{11}g.c. of exo-AAV9-CBA-GFP (self-complentary) was injected into BALB/c mice. After 3 weeks, the mice were perfused with 50ml of PBS (10mM phosphate buffer) and 50 ml of 4% PFA at a rate of 9ml/min, before injecting a solution of 2% gelatin (SIGMA G-1890) added with 0.02% of Dextran, Texas Red 75kDa in order to visualize the brain vasculature. The entire mice were then incubated for 15 minutes in ice for dissecting the brain and storing it in 4%PFA.

The brain was embedded in a 4.5% oxidized agarose block and was subsequently placed in a solution of 0.5% sodium borohydride in 0.5 M sodium borate buffer to covalently link the brain to the agarose (27). Imaging was achieved with the TissueCyte 1000 coupled to a Spectra Physics Mai-Tai HP operating at 920nm. A Nikon 16× 0.8 NA objective was used and in the XY plane sampling was 1.2 microns. A total of 852 optical planes with 5 micron spacing were taken to image the entire cerebellum. The emitted fluorescent light was separated into three spectral channels in order to isolate the Texas Red and GFP signals.

Histology and GFP expression

At four weeks post-injection of standard AAV-CBA-GFP or exo-AAV-CBA-GFP, mice were given an overdose of anesthesia and transcardially perfused with PBS and 4% PFA. The brain was removed, post-fixed in 4% formaldehyde in PBS for 48 h, cryoprotected for three days in 30% sucrose and then frozen in a dry ice/2-methylbutane bath for immunohistological analysis of tissue sections. Brains were cut on the coronal plane in 40 μm sections using a cryostat microtome. For the retina, eyecups were removed and placed into 4%PFA in PBS for 2 hours, then were cryopreserved in 15% sucrose overnight. After washing off sucrose, eyecups were placed into OCT media and were frozen in dry ice/isopentane bath. Cryosections were mounted on a glass slide and imaged with a Zeiss LSM 710 micros. Immunofluorescence was performed in free-floating sections with a primary antibody for GFP (chicken anti-GFP, Aves, 1:500), altogether with various other antibodies for cell types and sub-types. Briefly, the sections were permeabilized in PBS with Triton-X 0.5% for 2 h, blocked in 5% normal goat serum for 1 h, and incubated with the primary antibody overnight at 4°C. The sections were thoroughly washed in PBS, incubated with 1:1000 goat anti-chicken Alex Fluor 488-conjugated antibody (Cell Signaling, Danvers, MA) for 1 h at room temperature, washed again in PBS, and coverslipped with fluorescent mounting media containing DAPI (Dako, Carpinteria, CA).

Epifluorescence microscopy

Tile-scan images were collected on a Zeiss Axio Imager Z epifluorescence microscope equipped with AxioVision software and modified for automated acquisition of entire brain slices, using either 5×, 10× or 20× objectives. Exposure times for each specific

immunostaining were maintained unchanged between each slice imaged, in order to document differences in the transduction efficiency between AAV and exo-AAV.

Stereology-Based Quantitative Analyses

Stereology-based studies were performed as previously described (39), using a motorized stage of an Olympus BX51 epifluorescence microscope equipped with a DP70 digital CCD camera, an X-Cite fluorescent lamp, and the associated CAST stereology software version 2.3.1.5 (Olympus, Tokyo, Japan). Each cerebral area (respectively cortex, hippocampus and striatum) was initially outlined under the 4× objective in order to define the region of interest to scan. Random sampling of the selected area was defined using the optical dissector probe of the software. To evaluate the percentage of AAV9/exo-AAV9 transduced astrocytes or neurons, the stereology-based counts were performed under the 20× objective, with a meander sampling of 10% for the surface of cortex and striatum, and 30% for the hippocampus. For each counting frame, the total number of astrocytes (GS positive cells) or neurons (NeuN positive cells) were evaluated, and, among each of those populations, the GFP positive cells. Only glial and neuronal cells with DAPI-positive nucleus within the counting frame were considered. Counts were performed blindly. The density of astrocytes and of microglial cells was calculated as the number of cells of each type (+/− GFP positive cells), divided by the total area sampled (number of disectors × counting frame size).

Bioluminescence imaging

All imaging experiments were performed using the IVIS Spectrum imager outfitted with an XGI-8 gas anesthesia system (PerkinElmer, Waltham, MA). Mice which had previously been i.v. injected with either ss-AAV8-CBA-FLuc or ss-exo-AAV-FLuc were anesthetized and then injected intraperitoneally with 4.5 mg of D-luciferin substrate resuspended in 150 μl of PBS. Five minutes post-substrate injection, mice were imaged for luciferase expression using auto-acquisition. Region of interest were selected and imaging were analyzed using LivingImage software (v4.17,PerkinElmer).

Antibody evasion experiments

In vitro neutralization assays were performed with Gammagard S/D purified intravenous immunoglobulin (IVIg), (Baxter, Deerfield, IL, kindly provided by Dr. Luk H. Vandenberghe, Harvard Medical School). HeLa cells were seeded at 50,000 cells per well in a 96 well plate the day before the assay. Next, a dose of 5×10^8 g.c. of AAV8-FLuc or exo-AAV8-Fluc was mixed with serial dilutions of human serum or IVIg in FBS-free media to yield the indicated concentrations in the figure. AAV or exo-AAV with no human serum served as control. These were incubated for 1 h at 37°C before adding to cells for 1.5 h at 37°C. After washing cells one time, and replacing with complete medium, cells were incubated for 48 h before performing a luciferase assay using Bright-Glo™ Luciferase reagent (Promega, Madison, WI). Luciferase values for each sample, expressed in relative light units (RLUs) were plotted as a percentage of the AAV transduction sample without serum (which was set to 100%).

Ex-vivo luciferase assay and quantitative PCR for vector genomes

At the time post-vector injection indicated in the figure legend, mice were mice were given an overdose of anesthesia and transcardially perfused with cold PBS. Organs (liver, whole brain) were harvested for analysis of Fluc levels as well as virus genome copies (g.c.). Tissues were quickly removed from the animals, and immediately frozen on liquid nitrogen and stored at −80 °C.

For FLuc assay, 50 mg of each tissue was placed in 2 ml tubes containing 1.4 mm ceramic beads (Mo Bio Laboratories, Inc., Carlsbad CA) and 500 μL of Mammalian Protein Extraction Reagent (M-PER; Pierce Biotechnology, IL, USA). Tissues were homogenized in a BeadBug microtube homogenizer (Benchmark Scientific, Edison, NJ). Next, tubes were centrifuged for 5 minutes at 300 × g and 20 μL of tissue homogenate was transferred to 96-well white bottom plate and analyzed using 100 μL of Bright-Glo™ FLuc substrate reagent (Promega, WI, USA) and a plate luminometer (Dynex Technologies, VA, USA). A Bradford assay (Bio-Rad, Hercules, CA) was performed to normalize each FLuc value to the total amount of protein in the sample.

For the quantitative PCR assay to detect AAV genomes in organs, 25 mg of each organ was cut into small pieces using a sterile razor blade. Isolation of mouse genomic and AAV DNA was performed using the DNeasy® Blood and Tissue Handbook (Qiagen, Valencia, CA). Next 100 ng of total DNA was used as template for a quantitative TaqMan PCR that detects AAV genomes (Poly A region of the transgene cassette) as previously described (40).

bEnd.3 endothelial cell transwell assay

Cell culture inserts (Corning Incorporated, Durham, NC) featuring a transparent polyethylene terephthalate track-etched membrane with 3.0 μm pores designed for use in 24-well format cell culture plates were utilized for all transendothelial assays (41). Membranes were coated with rat-tail collagen type 1 (50 ug/ml), incubated for 1 hour at room temperature, then rinsed with 1X-PBS (Corning Incorporated). bEnd.3 cells (transformed BALB/c cortical endothelial cells) were plated at a density of 4×10^4 cells per insert and cultured in a humidified incubator supplemented with 5% CO_2 at 37°C until a confluent monolayer was established (20). Standard AAV or exo-AAV vectors were suspended in bEnd.3 media (see cell culture methods). A dose (1.6×10^{10} g.c.) of either conventional AAV or exo-AAV vectors was applied to the apical side of cell culture inserts (upper chamber), while vector-free bEnd.3 media was dispensed into the well below the inserts (lower chamber). After 24 hours of incubation, media was collected from the lower chamber and analyzed for the presence of vector particles by qPCR.

Statistics

Statistical analysis of data was performed using GraphPad Prism software (version 5.01). As indicated in the text, unparametric Mann Whitney tests were performed to compare the transduction efficacy of AAV9 with exo-AAV9. A value of $p< 0.05$ was considered to be statistically significant. For statistical analysis of bioluminescence assays, comparison between two groups was performed using an unpaired t test.

Supplementary Material

Refer to Web version on PubMed Central for supplementary material.

Acknowledgments

We thank Miguel Sena-Esteves for providing the AAV plasmids as well as Dr. David P. Corey for the expertise and resources of his laboratory on the cochlear transduction analysis. This work was supported by NIH/NINDS R21 NS081374-01 (CM), an American Brain Tumor Association Discovery grant (CM) and the Alzheimer's Drug Discovery Foundation (EH) and JPB Foundation (BTH). In addition, this work was also partially supported by NIH/NINDS R01 NS086570-01 (SHR). We would like to acknowledge the Nucleic Acid Quantitation Core at MGH Neuroscience Center for quantitative PCR analysis.

Conflict of Interest. CM has a patent application related to the Exo-AAV (vexosome) technology and has received royalty payments from agreements between Partners Healthcare and Exosome Diagnostics, Inc. CM has received an honorarium from Biogen Idec for giving a seminar on the technology.

REFERENCES

1. Kalia LV, Kalia SK, Lang AE. Disease-modifying strategies for Parkinson's disease. Mov Disord. 2015; 30(11):1442–1450. [PubMed: 26208210]
2. Muramatsu S. Gene therapy for Parkinson disease. Nihon Rinsho. 2010; 68(Suppl 8):646–649. [PubMed: 20976940]
3. Bennett J, Ashtari M, Wellman J, Marshall KA, Cyckowski LL, Chung DC, et al. AAV2 gene therapy readministration in three adults with congenital blindness. Sci Transl Med. 2012; 4(120): 120ra15.
4. Maguire AM, High KA, Auricchio A, Wright JF, Pierce EA, Testa F, et al. Age-dependent effects of RPE65 gene therapy for Leber's congenital amaurosis: a phase 1 dose-escalation trial. Lancet. 2009; 374(9701):1597–1605. [PubMed: 19854499]
5. Worgall S, Sondhi D, Hackett NR, Kosofsky B, Kekatpure MV, Neyzi N, et al. Treatment of late infantile neuronal ceroid lipofuscinosis by CNS administration of a serotype 2 adeno-associated virus expressing CLN2 cDNA. Hum Gene Ther. 2008; 19(5):463–474. [PubMed: 18473686]
6. Janson C, McPhee S, Bilaniuk L, Haselgrove J, Testaiuti M, Freese A, et al. Clinical protocol. Gene therapy of Canavan disease: AAV-2 vector for neurosurgical delivery of aspartoacylase gene (ASPA) to the human brain. Hum Gene Ther. 2002; 13(11):1391–1412. [PubMed: 12162821]
7. Yang B, Li S, Wang H, Guo Y, Gessler DJ, Cao C, et al. Global CNS transduction of adult mice by intravenously delivered rAAVrh.8 and rAAVrh.10 and nonhuman primates by rAAVrh.10. Molecular therapy : the journal of the American Society of Gene Therapy. 2014; 22(7):1299–1309. [PubMed: 24781136]
8. Foust KD, Nurre E, Montgomery CL, Hernandez A, Chan CM, Kaspar BK. Intravascular AAV9 preferentially targets neonatal neurons and adult astrocytes. Nat Biotechnol. 2009; 27(1):59–65. [PubMed: 19098898]
9. Gaj T, Epstein BE, Schaffer DV. Genome Engineering Using Adeno-associated Virus: Basic and Clinical Research Applications. Molecular therapy : the journal of the American Society of Gene Therapy. 2015
10. Swiech L, Heidenreich M, Banerjee A, Habib N, Li Y, Trombetta J, et al. In vivo interrogation of gene function in the mammalian brain using CRISPR-Cas9. Nat Biotechnol. 2015; 33(1):102–106. [PubMed: 25326897]
11. Tang W, Szokol K, Jensen V, Enger R, Trivedi CA, Hvalby O, et al. Stimulation-evoked Ca2+ signals in astrocytic processes at hippocampal CA3-CA1 synapses of adult mice are modulated by glutamate and ATP. J Neurosci. 2015; 35(7):3016–3021. [PubMed: 25698739]
12. Ekstrand MI, Nectow AR, Knight ZA, Latcha KN, Pomeranz LE, Friedman JM. Molecular profiling of neurons based on connectivity. Cell. 2014; 157(5):1230–1242. [PubMed: 24855954]
13. Xu W, Sudhof TC. A neural circuit for memory specificity and generalization. Science. 2013; 339(6125):1290–1295. [PubMed: 23493706]

14. Cai D, Cohen KB, Luo T, Lichtman JW, Sanes JR. Improved tools for the Brainbow toolbox. Nat Methods. 2013; 10(6):540–547.
15. Shimano T, Fyk-Kolodziej B, Mirza N, Asako M, Tomoda K, Bledsoe S, et al. Assessment of the AAV-mediated expression of channelrhodopsin-2 and halorhodopsin in brainstem neurons mediating auditory signaling. Brain Res. 2013; 1511:138–152. [PubMed: 23088961]
16. Kaspar BK, Vissel B, Bengoechea T, Crone S, Randolph-Moore L, Muller R, et al. Adeno-associated virus effectively mediates conditional gene modification in the brain. Proc Natl Acad Sci U S A. 2002; 99(4):2320–2325. [PubMed: 11842206]
17. Maguire CA, Balaj L, Sivaraman S, Crommentuijn MH, Ericsson M, Mincheva-Nilsson L, et al. Microvesicle-associated AAV vector as a novel gene delivery system. Molecular therapy : the journal of the American Society of Gene Therapy. 2012; 20(5):960–971. [PubMed: 22314290]
18. Balaj L, Atai NA, Chen W, Mu D, Tannous BA, Breakefield XO, et al. Heparin affinity purification of extracellular vesicles. Scientific reports. 2015; 5:10266. [PubMed: 25988257]
19. Gyorgy B, Fitzpatrick Z, Crommentuijn MH, Mu D, Maguire CA. Naturally enveloped AAV vectors for shielding neutralizing antibodies and robust gene delivery in vivo. Biomaterials. 2014; 35(26):7598–7609. [PubMed: 24917028]
20. Hawkins BT, Grego S, Sellgren KL. Three-dimensional culture conditions differentially affect astrocyte modulation of brain endothelial barrier function in response to transforming growth factor beta1. Brain Res. 2015; 1608:167–176. [PubMed: 25721792]
21. Kotin RM. Large-scale recombinant adeno-associated virus production. Hum Mol Genet. 2011; 20(R1):R2–E6. [PubMed: 21531790]
22. Zhang H, Xie J, Xie Q, Wilson JM, Gao G. Adenovirus-adeno-associated virus hybrid for large-scale recombinant adeno-associated virus production. Hum Gene Ther. 2009; 20(9):922–929. [PubMed: 19618999]
23. de Rivero Vaccari JP, Brand F 3rd, Adamczak S, Lee SW, Barcena JP, Wang MY, et al. Exosome-mediated inflammasome signaling after central nervous system injury. J Neurochem. 2015
24. Rajendran L, Bali J, Barr MM, Court FA, Kramer-Albers EM, Picou F, et al. Emerging roles of extracellular vesicles in the nervous system. J Neurosci. 2014; 34(46):15482–15489. [PubMed: 25392515]
25. Pegtel DM, Peferoen L, Amor S. Extracellular vesicles as modulators of cell-to-cell communication in the healthy and diseased brain. Philos Trans R Soc Lond B Biol Sci. 2014; 369(1652)
26. Volterra A, Liaudet N, Savtchouk I. Astrocyte Ca(2)(+) signalling: an unexpected complexity. Nat Rev Neurosci. 2014; 15(5):327–335. [PubMed: 24739787]
27. Ragan T, Kadiri LR, Venkataraju KU, Bahlmann K, Sutin J, Taranda J, et al. Serial two-photon tomography for automated ex vivo mouse brain imaging. Nat Methods. 2012; 9(3):255–258. [PubMed: 22245809]
28. Bemelmans AP, Duque S, Riviere C, Astord S, Desrosiers M, Marais T, et al. A single intravenous AAV9 injection mediates bilateral gene transfer to the adult mouse retina. PLoS One. 2013; 8(4):e61618. [PubMed: 23613884]
29. Luebke AE, Rova C, Von Doersten PG, Poulsen DJ. Adenoviral and AAV-mediated gene transfer to the inner ear: role of serotype, promoter, and viral load on in vivo and in vitro infection efficiencies. Adv Otorhinolaryngol. 2009; 66:87–98. [PubMed: 19494574]
30. Wood MJ, O'Loughlin AJ, Samira L. Exosomes and the blood-brain barrier: implications for neurological diseases. Ther Deliv. 2011; 2(9):1095–1099. [PubMed: 22833906]
31. Alvarez-Erviti L, Seow Y, Yin H, Betts C, Lakhal S, Wood MJ. Delivery of siRNA to the mouse brain by systemic injection of targeted exosomes. Nat Biotechnol. 2011; 29(4):341–345. [PubMed: 21423189]
32. Lai CP, Mardini O, Ericsson M, Prabhakar S, Maguire CA, Chen JW, et al. Dynamic biodistribution of extracellular vesicles in vivo using a multimodal imaging reporter. ACS Nano. 2014; 8(1):483–494. [PubMed: 24383518]
33. Hareendran S, Balakrishnan B, Sen D, Kumar S, Srivastava A, Jayandharan GR. Adeno-associated virus (AAV) vectors in gene therapy: immune challenges and strategies to circumvent them. Rev Med Virol. 2013; 23(6):399–413. [PubMed: 24023004]

34. Rogers GL, Martino AT, Aslanidi GV, Jayandharan GR, Srivastava A, Herzog RW. Innate Immune Responses to AAV Vectors. Front Microbiol. 2011; 2:194. [PubMed: 21954398]

35. Gray SJ, Matagne V, Bachaboina L, Yadav S, Ojeda SR, Samulski RJ. Preclinical differences of intravascular AAV9 delivery to neurons and glia: a comparative study of adult mice and nonhuman primates. Molecular therapy : the journal of the American Society of Gene Therapy. 2011; 19(6): 1058–1069. [PubMed: 21487395]

36. Hudry E, Van Dam D, Kulik W, De Deyn PP, Stet FS, Ahouansou O, et al. Adeno-associated virus gene therapy with cholesterol 24-hydroxylase reduces the amyloid pathology before or after the onset of amyloid plaques in mouse models of Alzheimer's disease. Molecular therapy : the journal of the American Society of Gene Therapy. 2010; 18(1):44–53. [PubMed: 19654569]

37. Hudry E, Dashkoff J, Roe AD, Takeda S, Koffie RM, Hashimoto T, et al. Gene transfer of human Apoe isoforms results in differential modulation of amyloid deposition and neurotoxicity in mouse brain. Sci Transl Med. 2013; 5(212):212ra161.

38. Spires TL, Meyer-Luehmann M, Stern EA, McLean PJ, Skoch J, Nguyen PT, et al. Dendritic spine abnormalities in amyloid precursor protein transgenic mice demonstrated by gene transfer and intravital multiphoton microscopy. J Neurosci. 2005; 25(31):7278–7287. [PubMed: 16079410]

39. Serrano-Pozo A, Muzikansky A, Gomez-Isla T, Growdon JH, Betensky RA, Frosch MP, et al. Differential relationships of reactive astrocytes and microglia to fibrillar amyloid deposits in Alzheimer disease. J Neuropathol Exp Neurol. 2013; 72(6):462–471. [PubMed: 23656989]

40. Maguire CA, Crommentuijn MH, Mu D, Hudry E, Serrano-Pozo A, Hyman BT, et al. Mouse gender influences brain transduction by intravascularly administered AAV9. Molecular therapy : the journal of the American Society of Gene Therapy. 2013; 21(8):1470–1471. [PubMed: 23903572]

41. Persidsky Y, Fan S, Dykstra H, Reichenbach NL, Rom S, Ramirez SH. Activation of Cannabinoid Type Two Receptors (CB2) Diminish Inflammatory Responses in Macrophages and Brain Endothelium. J Neuroimmune Pharmacol. 2015; 10(2):302–308. [PubMed: 25666933]

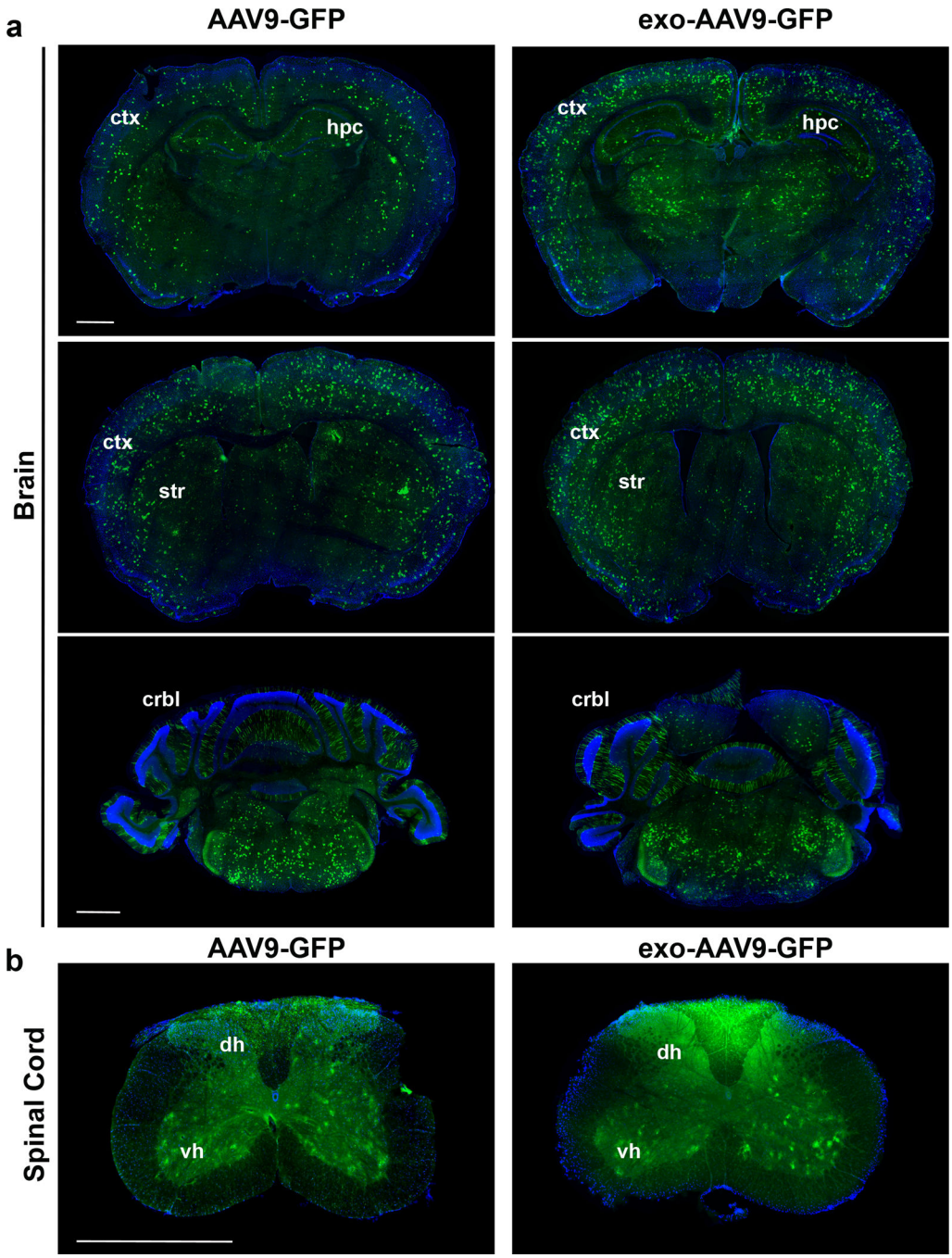

Figure 1. Overview of the distribution of GFP throughout the central nervous system (CNS) after i.v. injection of AAV9-CBA-GFP and exo-AAV9-CBA-GFP

Representative images of GFP fluorescence over three different coronal sections across the brain (**a**) and of the spinal cord (**b**) after intravenous injection of the same self-complementary genome vector copy (g.c.) numbers (1.5×10^{11} g.c.) of AAV9 (left panels) and exo-AAV9 (right panel). A widespread signal was observed for both vectors within the cortex (ctx), hippocampus (hpc), striatum (str) and cerebellum (crbl). Within the spinal cord,

GFP transduced cells could be observed in the ventral (vh) and dorsal (dh) horns. Scale bar: 1000μm.

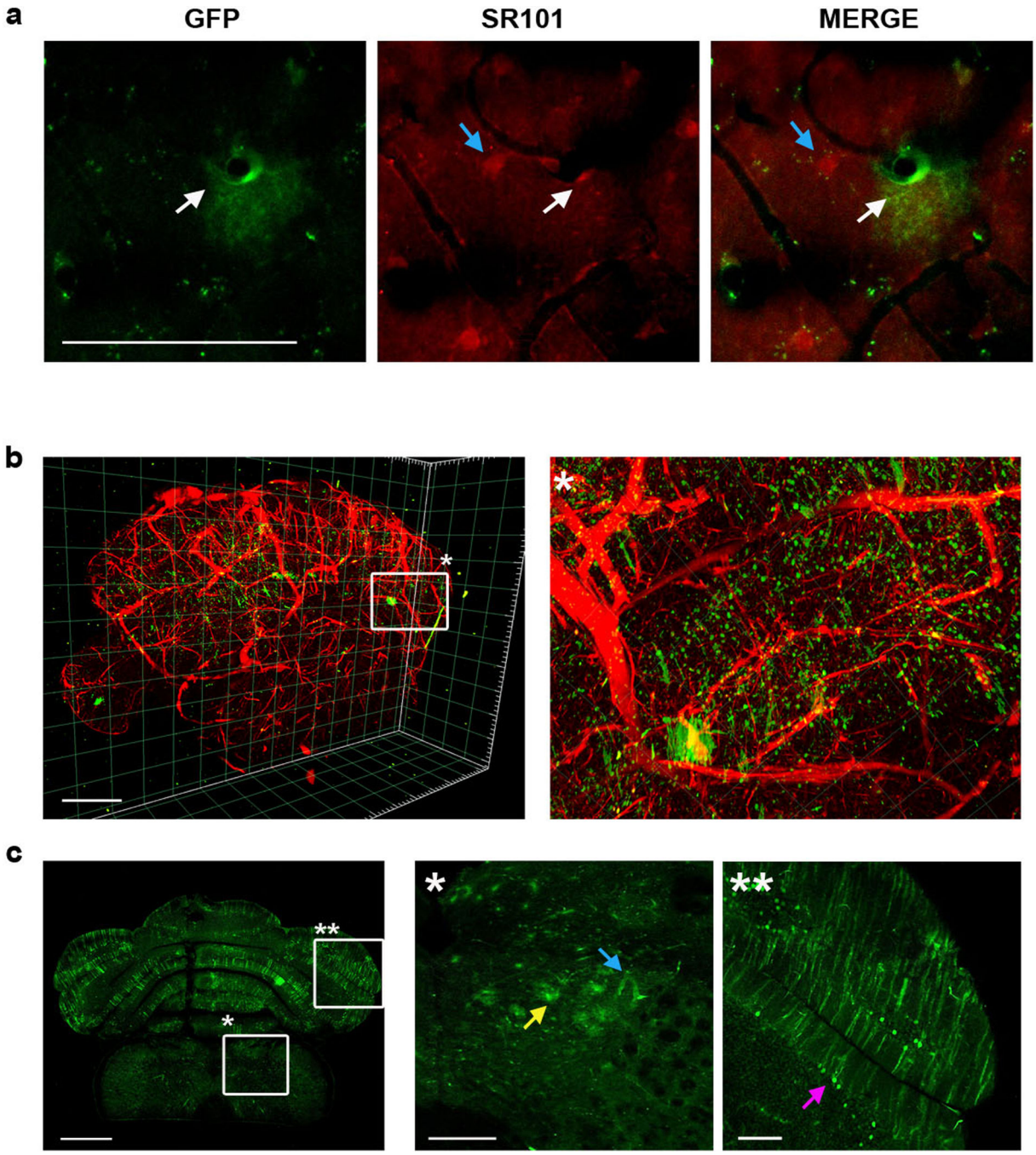

Figure 2. Detection of direct GFP fluorescence by *in vivo* two-photon imaging and *ex vivo* serial two-photon tomography (STP)

BALB/c mice were injected with 7×10^{11} g.c. of exo-AAV9-CBA-GFP. After 3 weeks, the GFP fluorescent signal was detected *in vivo* by multiphoton imaging or ex vivo by STP (in absence of immunostaining). (**a**) Representative 2-photon images of a GFP transduced astrocyte (white arrow, identified with the astrocytic marker SR101 topically applied on the brain) in the living animal after cranial window implantation. Numerous surrounding astrocytes do not express detectable GFP (blue arrow). Scale bar: 100μm. (**b**) Three-

dimensional reconstruction of the entire cerebellum by post-mortem STP tomography imaging, showing the whole vascular tree as well as the direct fluorescent signal across this particular region of the brain. On the right panel, numerous GFP transduced cells could be identified on a higher magnification image of a small region of the cerebellum. Scale bar: 1000μm (**c**) GFP signal detected in one section of the cerebellum imaged by 2-photon before 3D-reconstruction. Scale bar: 1000μm. On the right, two cropped regions of the initial image show GFP positive astrocytes (yellow arrow), vascular endothelium (blue arrow) and Purkinje cells (purple arrow). Scale bar: 200μm.

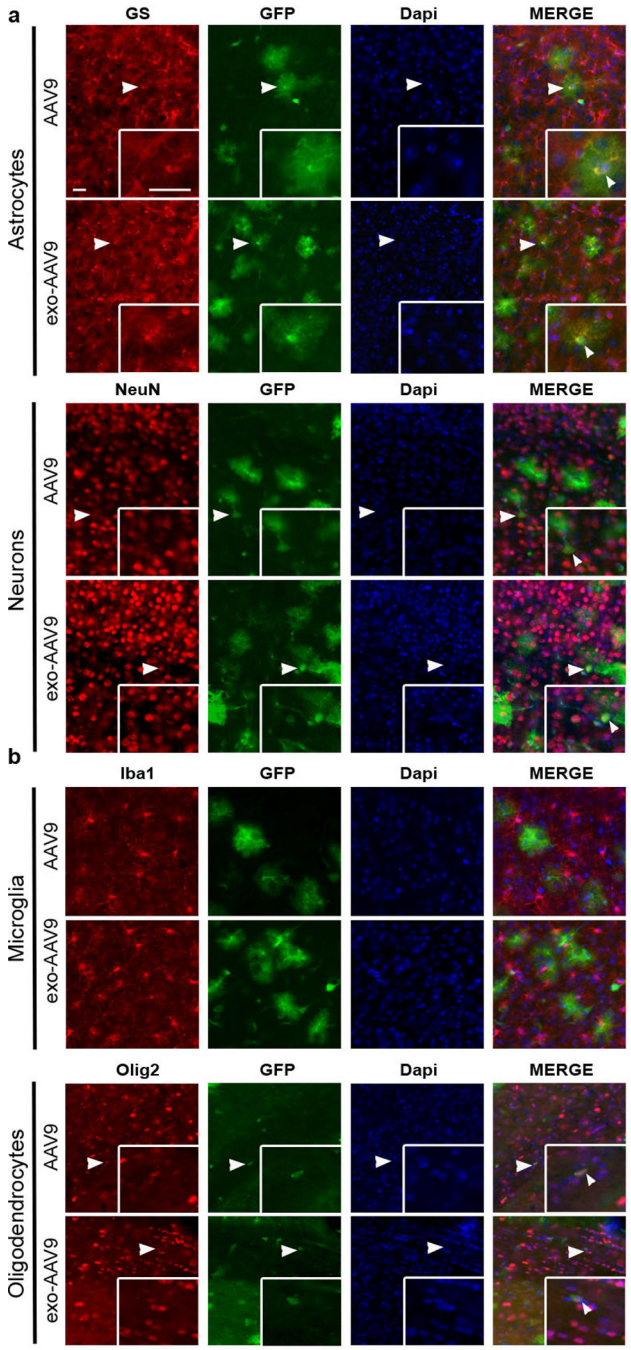

Figure 3. Astrocytes and neurons as preferentially targeted by peripherally administered AAV9 and exo-AAV9

Double immunostainings were performed in order to determine the main neural cell types transduced by both exo-AAV9 and AAV9 (white arrows). (**a**) Representative images of GFP positive astrocytes and neurons, respectively identified by the markers Glutamine synthetase (GS) and NeuN, in the cortex of injected mice. Astrocytes and neurons were predominantly transduced in the brain. (**b**) By contrast, no microglial cells (identified by Iba1 labeling) and rare oligodendrocytes (expressing Olig2) were observed. Scale bar: 50μm

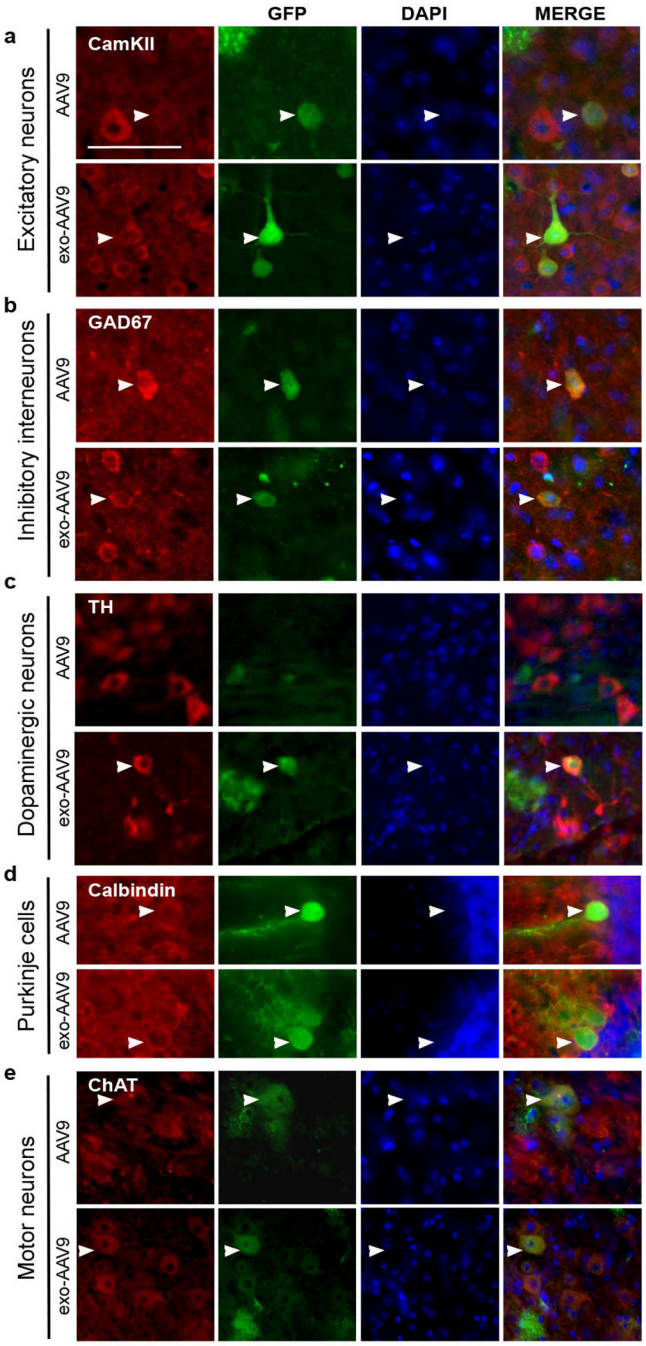

Figure 4. Neuronal sub-types transduced after peripheral injection of AAV9 and exo-AAV9

Representative images of co-labeling experiments performed to characterize the transduction profile of peripherally injected exo-AAV9 and AAV9 in various neuronal sub-types. The colocalization between GFP with CamKII (**a**) or GAD67 (**b**) markers demonstrates efficient targeting of excitatory and inhibitory neurons, respectively. (**c**) Interestingly, few GFP/Tyrosine hydroxylase (TH) positive dopaminergic neurons were observed after exo-AAV9 injection, but not with conventional AAV9. (**d**) In the cerebellum, numerous Purkinje cells, identified with the marker calbindin, express GFP after AAV9 and exo-AAV9 transduction.

(**e**) In the spinal cord, GFP positive motor neurons expressing the choline acetyltransferase (ChAT) were observed. Scale bar: 50μm.

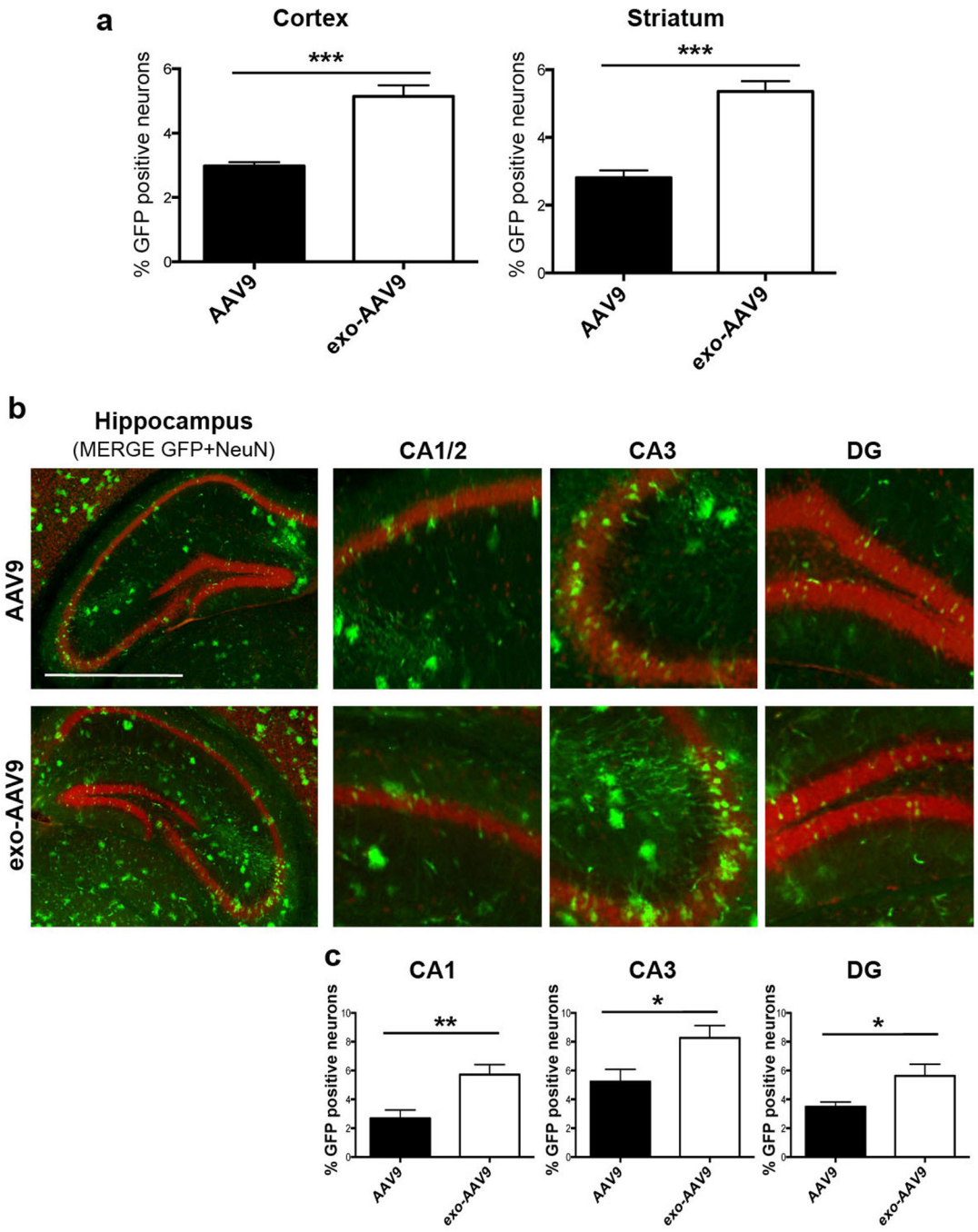

Figure 5. Stereology-based study of the percentage of AAV9 and exo-AAV9 transduced neurons

BALB/c mice were sacrificed 4 weeks after intravenous injection of 1.5×10^{11} g.c of conventional AAV9 or exo-AAV9. To evaluate the percentage of neuronal transduction, an unbiased stereological analysis of the total number of neurons (identified using the NeuN marker) and of the total number of transduced neurons (NeuN/GFP double positive cells) was achieved by random sampling of the cortex, striatum and hippocampus, following the protocol detailed in the Materials and Methods section. (**a**) GFP positive neurons were evenly distributed across the cortex (left panel) and the striatum (right panel) and showed a

significant increased percentage of transduction after exo-AAV9 administration (cortex: 5.11±0.28%; striatum: 5.31±0.27%) as compared with AAV9 (cortex: 2.87±0.12%; striatum: 2.79±0.18%). (**b**) By contrast, transduction variability was observed in the hippocampus, with both CA3 and the dentate gyrus (DG) being preferentially targeted by AAV9 and exo-AAV9 as compared with CA1–2. The mice injected with exo-AAV9 presented a higher density of NeuN/GFP neurons in each hippocampal sub-division than AAV9 (for AAV9: CA1/2: 2.66±0.46%; CA3: 4.37±0.84% and DG: 3.15±0.34% and for exo-AAV9: CA1/2: 5.45±0.57%; CA3: 7.93±0.54% and DG: 6.19±0.79%). n= 4 mice per group (3 sections analyzed per mouse); non-parametric Mann Whitney test; ***$p<0.0001$; **$p<0.005$; *$p<0.5$. Scale bar: 100μm

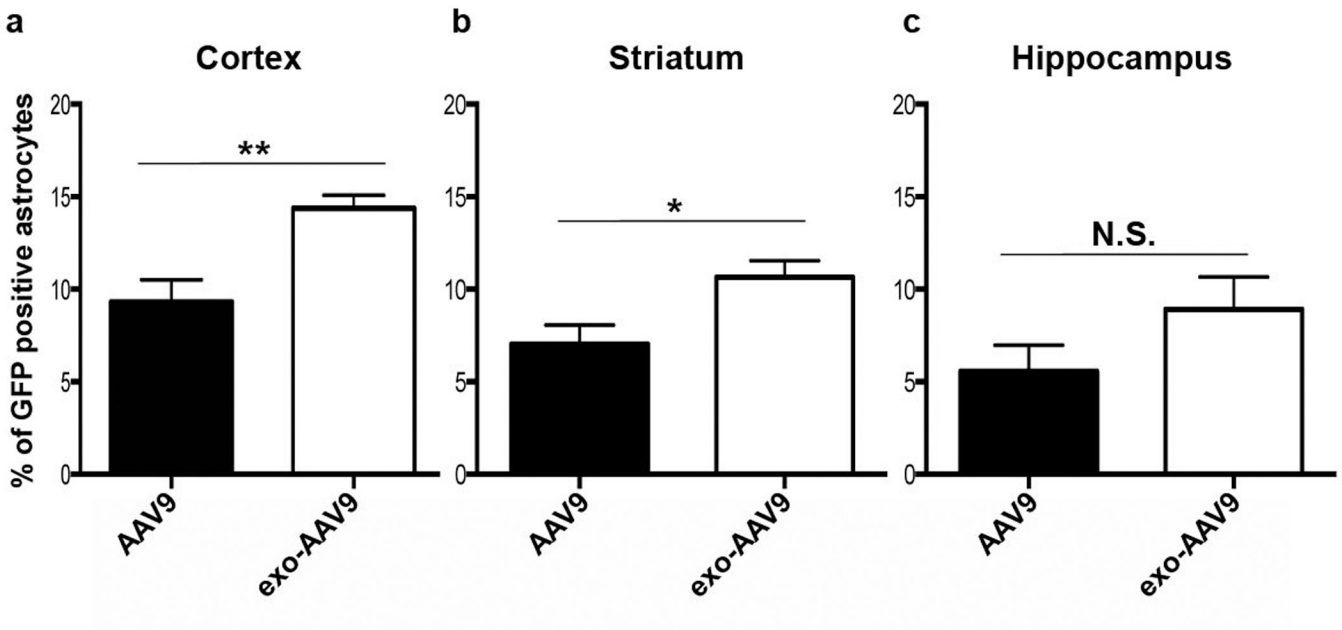

Figure 6. Stereology-based study of the percentage of AAV9 and exo-AAV9 transduced astrocytes

BALB/c mice were sacrificed 4 weeks after intravenous injection of 1.5×10^{11} g.c of conventional AAV9 or exo-AAV9. To evaluate the percentage of transduced astrocytes, an unbiased stereological analysis of the total number of astrocytes (identified Glutamine synthetase positive cells) and of the total number of transduced astrocytes (GS/GFP double positive cells) was achieved by random sampling of the cortex, striatum and hippocampus, following the protocol detailed in the Materials and Methods section. The percentage of GFP positive astrocytes was significant higher after i.v. injection of exo-AAV9 as compared with AAV9 in both cortex (**a:** AAV9: 9.3±1.2% and exo-AAV9: 15.37±0.7%) and striatum (**b**: AAV9: 7.02±1.05% and exo-AAV9: 12.64±0.91%). However, the difference did not reach significance in the hippocampus (**c**: AAV9: 5.56±1.41% and exo-AAV9: 8.91±1.74%). n= 4 mice per group (3 sections analyzed per mouse); non-parametric Mann Whitney test; **p<0.0001; **p<0.005; *p<0.5.

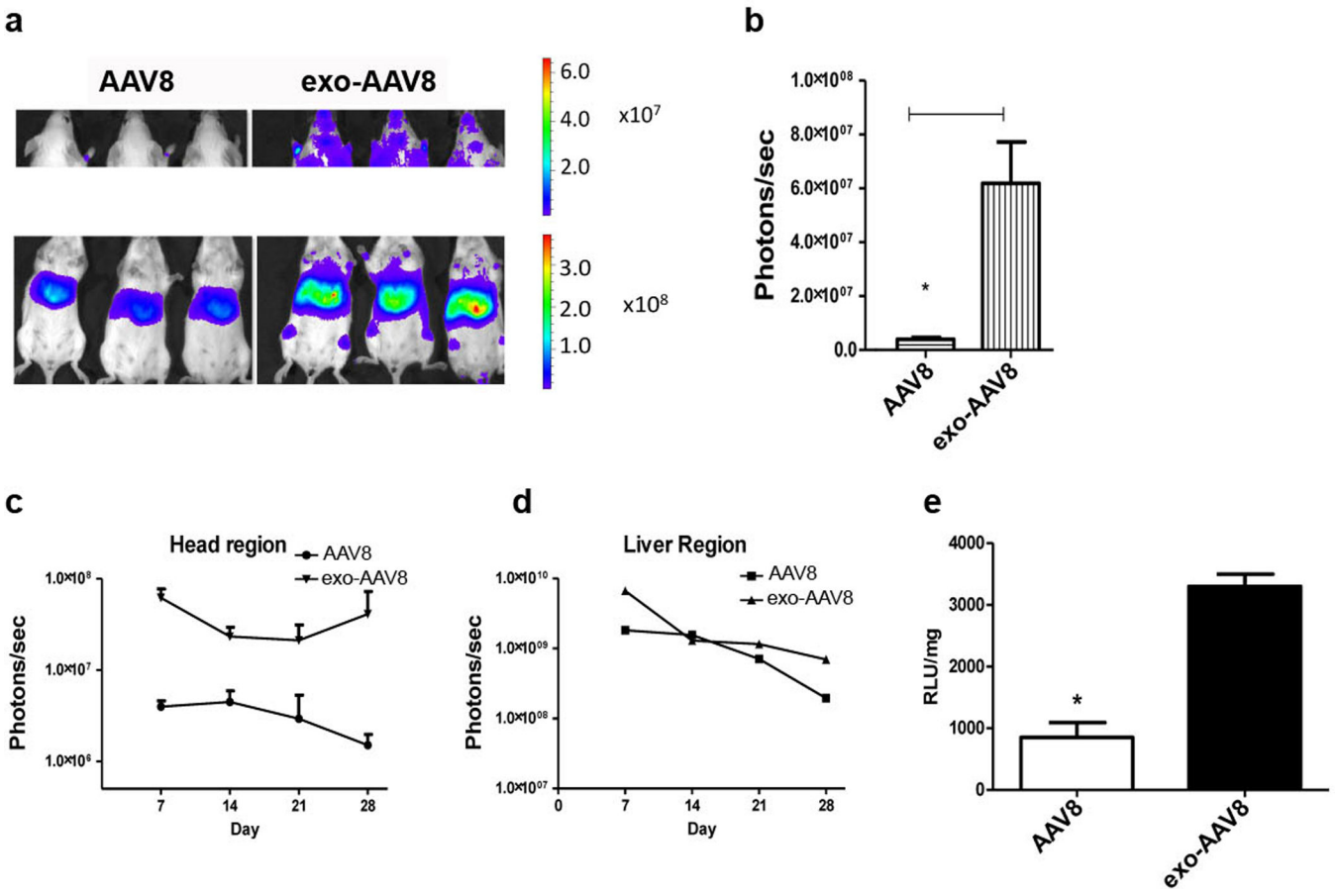

Figure 7. Kinetics of exo-AAV8 and standard AAV8 luciferase (FLuc) expression after systemic injection

BALB/c mice were injected i.v. with 5×10^{10} g.c. of either standard AAV8-FLuc or exo-AAV8-FLuc. (**a**) Representative images of bioluminescence intensity of head and liver region in mice 7 days post-injection for AAV8 and exo-AAV8. (**b**) Bioluminescent signal quantitation in head region one week post injection. Kinetics of FLuc bioluminescence over 4 weeks in head (**c**) and liver (**d**) region. (**e**) Luciferase levels in brain homogenates isolated from mice injected i.v. with AAV8-FLuc or exo-AAV8-FLuc.

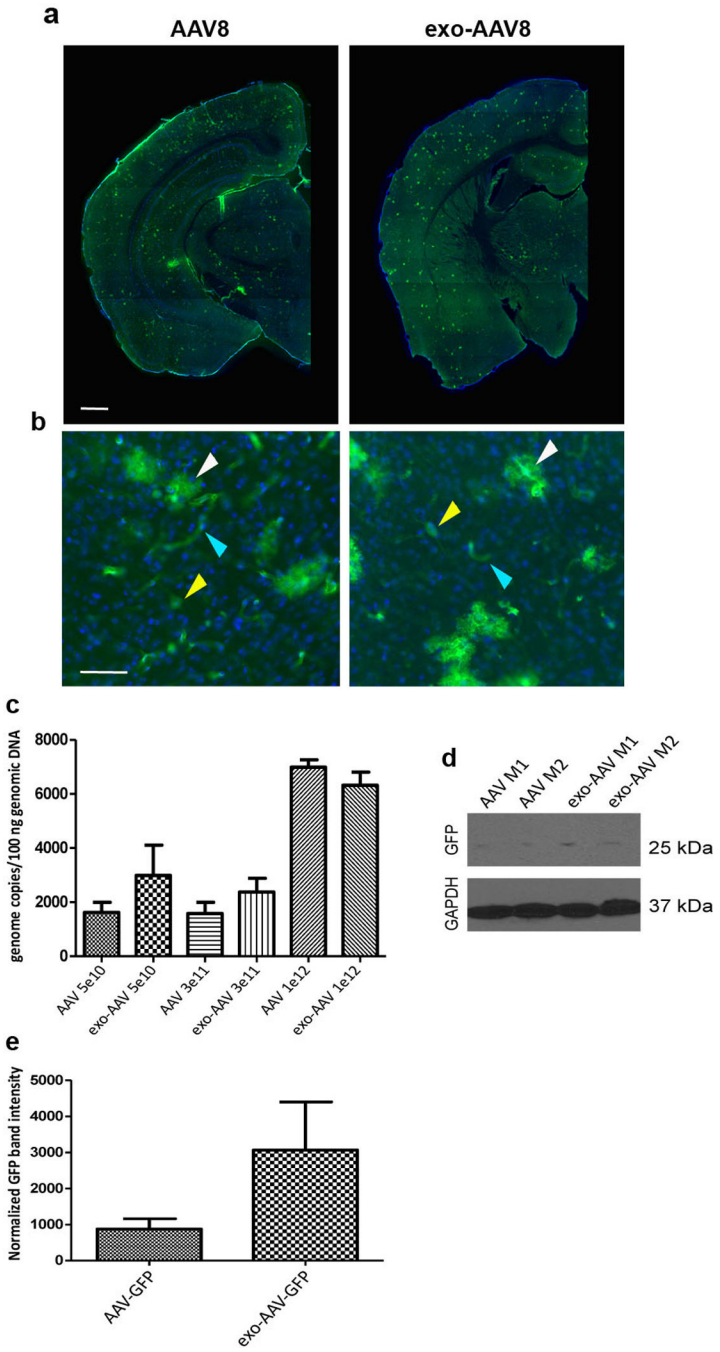

Figure 8. exo-AAV8 enhances GFP reporter expression over standard AAV8 at low vector doses

(**a**) BALB/c mice were injected i.v. with 4×10^{11} g.c. of either AAV8 (left panels) or exo-AAV8 (right panels) constructs and two weeks later, sacrificed, and cryosections immunostained with an anti-GFP antibody. Representative images of a coronal section after immunostaining show no difference in the intensity of GFP signal between both vectors (upper panels). Scale bar: 1000μm. At higher magnification (**b**), transduced cells with morphological features of astrocytes (white arrows), neurons (yellow arrows) as well as cerebral vasculature (blue arrows) could be detected. Scale bar: 100μm. (**c**) In order to

decipher the discrepancy between our GFP and Luc data, BALB/c mice were then injected i.v. with the indicated doses of single-stranded AAV8-GFP or exo-AAV8-GFP. Two weeks post injection mice were sacrificed and genomic and virus vector DNA isolated and subjected to an AAV-specific qPCR. n=2 per dose. (**d**) Brain homogenates of mice injected at the lowest dose (5×10^{10} g.c.) were subjected to immunoblot detection of GFP. GAPDH was shown as loading control. M1 and M2 refer to two separate animals in each group (mouse 1 and mouse 2) analyzed for GFP expression. (**e**) Densitometry was performed on GFP bands and normalized to the GAPDH bands.

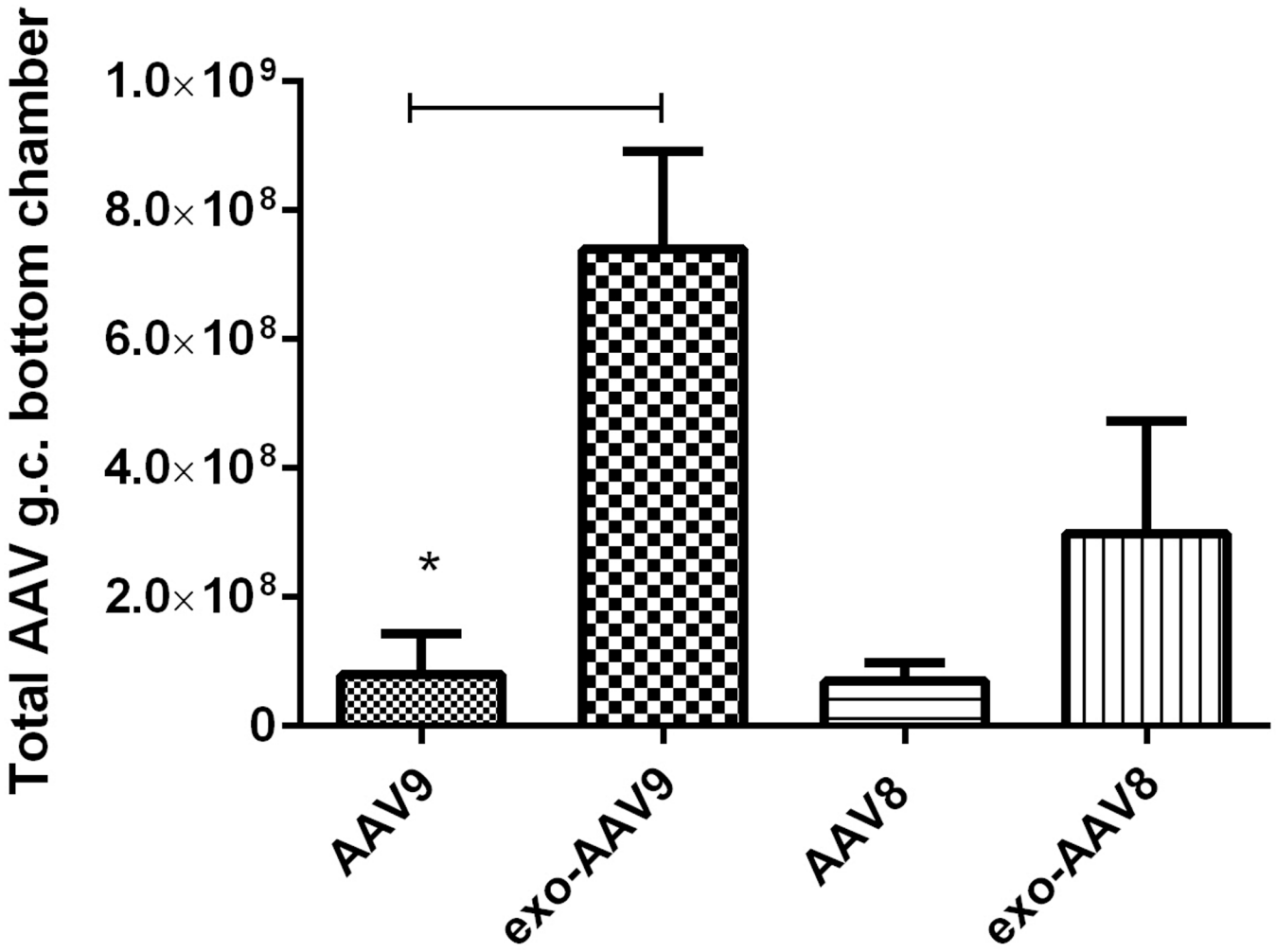

Figure 9. exo-AAV cross a blood-brain barrier model

bEnd.3 cells, a cell line generated from mouse cortical endothelial cells, were seeded on cell culture inserts and grown to confluence in order to establish an *in vitro* blood-brain barrier model. Standard AAV or exo-AAV (1.6×10^{10} genome copies) were suspended in media and dispensed into the upper chamber (apical side of cell culture inserts), while vector-free media was added to the lower chamber (below the inserts). After 24 hours, media was collected from the lower chamber to determine the number of AAV genomes present in the media by qPCR. (**a**) Data are presented as the mean of total AAV genome copies below the cell culture insert ± standard deviation. n=4 transwell assays per group; t-test between standard AAV and exo-AAV for each serotype; *$p<0.05$.